Anonymous Referee #1

Received and published: 19 Mars 2018

Comments from Referee 1:

The article deals with the problem of landslides (rockslide) based on both monitoring and numerical approaches. The article is composed of two parts. The first part is dedicated to the description of the physical problem, the engineering geological properties and the monitoring results. After a successful prediction for an excavation-induced rockslide in 2011, the monitoring system is proven to be suitable to the rainfall-induced rockslide. The second part of the article deals with numerical analysis (using an advanced numerical method, FEMLIP) of the stability problem. The stability is analyzed using the so called second-order work criterion, and a safety factor from numerical calculation is compared with the monitoring data. This paper is convincing and valuable in light of very interesting monitoring system and a deep comparison between in situ measurements and the advanced computational results. I would recommend publication once after the manuscript has been modified according to the comments provided below.

Specific comments and questions:

- Fig. 5b should be explained. Why the CR-forces are different?

Author's response:

Thanks for your kindly reminder. The CR-forces in Fig. 5b were obtained from the CRLD cables with different specifications. The CR-force is determined by several factors, such as the geometry of the pipe and cone, the frictional coefficient on the pipe-cone interface, the material property of the components and so on. With the elastic assumption, the CR-force can be estimated by the expression as shown in Fig.1 [1].

where P is the CR-force, f is the frictional coefficient on the pipe-cone interface, I_s and I_c are the geometrical and elastic parameters, respectively.

Comments from Referee 1:

- p.7, l.1: The author said that ". . .have proposed several successful predictions for rockslides occurred in this zone". All these monitoring data have to be considered as "Big Data", or they can be managed in a usual way without considering an "ad hoc" software to detect some anomalous measurements? In the future, probably some specific Big Data treatments will be necessary.

Author's response:

The monitoring system provides the real-time monitoring data, and sends early warnings according to the increase of the anchorage force. Although we have already quite a few monitoring data, it cannot be considered as a "big data" treatment, which requires much more data to propose reliable predictions.

Comments from Referee 1:

- How anchors are placed in the rock: inclination, depth, etc. What are the criteria that determine these parameters?

Author's response:

The anchors are placed in the rock generally with an inclination of 25° and a depth of 50-80m. The depth of the CRLD cable depends on the orientation of potential sliding band, such as the fault. The inclination is 25^{o} because it is easy to install the sleeve pipe and the cone.

Comments from Referee 1:

- I did not understand how the triggering point of the warning system is determined. It is very difficult to discriminate the onset of a slow/gradual sliding and a sudden/quick sliding prior to global failure. This point deserves more discussions.

Author's response:

You are perfectly correct. Our warning triggers are determined, based on a large number of applications in rock slopes. From the stable stage (the anchorage force is constant), if the anchorage force increases 400kN, the yellow warning will be sent, and then, once it increases 300 kN, the orange and red warning will be sent, orderly. Certainly, this is a qualitative prediction, and the in-situ observation is also needed.

Comments from Referee 1:

- The authors claim that the measuring system is suitable for rockslides due to different triggering factors (excavation, rainfall, etc.). Is it suitable for other types of material? For example, the soil slopes.

Author's response:

Thanks for your question. Indeed, this measuring system was developed initially for rock slopes in open-pit mines, especially in which sliding might occur along certain weak zone (fault, joint, etc). It has been applied in 15 regions in China, with more than 200 monitoring points, and empirical warning criterion has also been obtained according to statistical method. In addition, recently, it has also been used in a soil slope located at Dandong, China.

Comments from Referee 1:

- p.14, l.7 Give some explanations about the numerical infiltration process modeling.

Author's response:

Thanks for your question. The FEMLIP method used in this study can solve the full hydro-mechanical coupling, according to the previous contributions [2, 3]. The formulations in the global calculation are written as shown in Fig.2. The detail of the formations can be referred to the papers [2, 3]. With the water flux q = 24 mm/h considered in the simulation, the velocity and water pressure fields could be calculated in the grid points and interpolated into material points according to the shape function, at each time step. With the strain and the water pressure in the material points, the stress and the degree of saturation were refreshed according to the constitutive model, presented in the manuscript.

Anonymous Referee #2

Received and published: 11 December 2018

Comments from Referee 2:

Dear Editor and Authors, This paper addresses the issue of monitoring of rocky slope instability and failure analysis using the FEMLIP method, and the normalized global second order work as failure index. The paper is innovative in terms of methods and tools and provides useful results for the efficiency of the monitoring and the numerical analysis of rock slides, as tools for the prediction and simulation of failure and the early warning. The methods used and the results are clearly explained. Figures are sufficient, although the quality can be improved (please check comments on the pdf file for Figure 2b).

Author's response:

Thanks so much for your pertinent comments. The 2 figures you pointed out had been substituted, and the resolution had been improved.

Author's changes in manuscript:

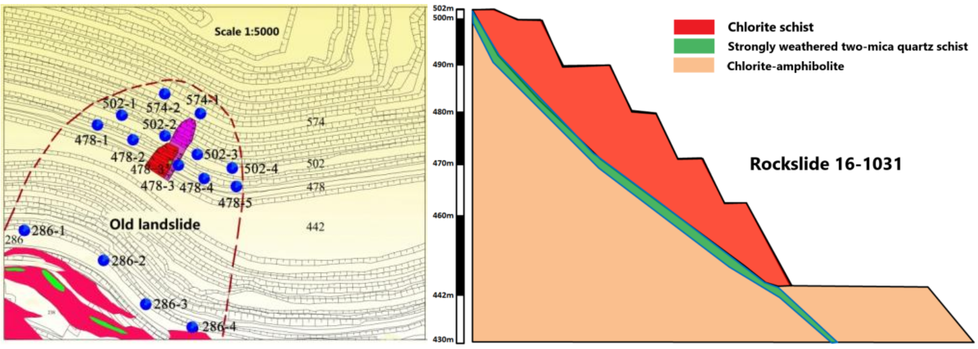

Comments from Referee 2:

I would suggest a thorough review of the English style, as some parts need to be rephrased in order to be correct and clear.

Author's response and author's changes in manuscript:

You are reasonable. A thorough review will be performed.

Comments from Referee 2:

In terms of methodology and concepts I would like to raise the issue of rock bridges and their failure. The Authors claim that failure occurs along the strongly weathered two-mica quartz schist, which is simulated as continuous in the numerical model. However i in rockslides the occurrence of failure through the breakage of intact rock bridges is quite common. This has not been taken into account in the numerical analysis. How do the Authors deal with this, in this work?

Author's response and author's changes in manuscript:

Thanks very much for your question, and you are reasonable. The stability of the engineering rock mass is generally determined by the rock blocks and the geological discontinuities. The instability of rock slopes usually proceeds with the breakage of intact rock bridges, and then the global sliding. A consideration of the discontinuous phenomenon into the FEMLIP method is interesting, and this is effectively an ongoing work. We are trying to implementing level-set functions to describe it, but now the FEMLIP method cannot yet solve this issue. In conclusion, this issue will be presented as a shortcoming and a perspective of this study.

According to the geological data, the failure occurs principally along the two-mica quartz schist, which is highly fragmented presenting as blocks and debris and filled with mud. Hence, we considered it as granular material, and simulated it as continuous medium. In addition, based on the mechanical parameters of the rock bridges and the fissures, their weighted average values can be used as the mechanical parameters of the weak zone [4, 5]. In this work, the involved mechanical parameters are reduced in line with the empirical strength reduction method.

Author's changes in manuscript:

In addition, the instability of rock slopes usually proceeds with the breakage of intact rock bridges. The description of this discontinuous phenomenon using the FEMLIP method is worth being considered. By implementing the level-set functions, widely used in X-FEM, the FEMLIP method can be extended to solve the issues of discontinuous media.

Please find more comments on the .pdf file. Kind regards

The comments on the PDF file are responded as follows:

Comments from Referee 2:

P.1 L.14, correct "was" as "were"

Author's response and author's changes in manuscript:

Thanks so much, and it has been modified in the manuscript.

Comments from Referee 2:

P.1 L.16, I think this sentence "and the normalized global second order work was implanted to assess the structure instability as a safety factor" should be rephrases

Author's response and author's changes in manuscript:

You are reasonable, and this sentence is rephrased as "and two forms of the normalized global second order work were calculated to analyze the stability of the rock slope". Is it OK?

Comments from Referee 2:

P.2 L.16, It would be interesting to know more about the monitoring system that was used.

Author's response and author's changes in manuscript:

You are right, more details about the monitoring system will be added in the manuscript.

Comments from Referee 2:

P.4 L.3, resolution needs to be improved.

Author's response and author's changes in manuscript:

Thanks for your kindly reminder, and it has been replaced by one with a higher resolution.

Comments from Referee 2:

P.4 L.10, It would be better to use a legend. Also the resolution of figure 2b needs to be improved.

Author's response and author's changes in manuscript:

Thanks for your kindly reminder. A legend has been added and the resolution improved.

Comments from Referee 2:

P.6 L.19, How is the depth of the anchored end into the rock, determined? How is it guaranteed that it is anchored on a fixed end?

Author's response:

The CRLD cables are generally installed in the rock mass with an inclination of 25^{o} and the depth depends on that of the potential sliding band, such as the weak zone. As the monitoring system is used principally for rock slopes, the weak zone is determined by boreholes. The fixed end should be anchored into the stable rock, under the weak zone. About the installation of the CRLD cables in rock mass, more details can be found in the paper [6].

Comments from Referee 2:

P.7 L.14, In how much time was this increase observed? What was the monitoring time interval before?

Author's response:

Thanks very much for your careful review! Regarding the monitoring results, it is not written clearly, and a detailed explanation has been made in the manuscript. The increase was observed from the initial installation of the monitoring system to the current time. The monitoring frequency is once per hour before the long term warning, and twice per hour after it. After the medium and short term warnings, the monitoring frequency should be doubled.

Author's changes in manuscript:

From September 7, 2015, the anchorage force monitored at point 478-3 showed a series of slow increases and three sudden increases, which accumulated a force increase from 270kN to 600kN until September 1, 2016, as remarked by the points A, B and C in Fig. 7a. Before September 1, 2016, the cumulative value had not strictly reached the warning threshold proposed by He (2009), and no obvious fissures were observed according to in-situ surveys; therefore, no warning was sent. As a result of constant mining activity, the cumulative increase of anchorage force reached 330 kN and the fourth sudden increase appeared after September 1, 2016, as remarked by the point D in Fig. 7a. Although no fissures were observed, the first long-term warning was sent due to the sudden increase by the field staff, and the monitoring frequency was increased to twice per hour. When the anchorage force returned to constant on October 1, 2016, the cumulative force increase exceeded 220 kN and a few surface fissures appeared, the medium term warning was sent. The mining activities were ceased and the monitoring frequency was doubled to 4 times per hour. In the following days, the curve remained constant and no obvious fissures continued to develop; therefore, mining excavations restarted along the bench at 442 m elevation on October 28, 2016. On October 30, the anchorage force suddenly increased again at 04:53, and reached a peak value of 855 kN at 17:07, during a period of rainfall. A subsequent dive of the anchorage force was observed. The short term warning was sent at 08:56 on October 31, and all staff was urgently evacuated. At 23:52 on October 31, the rockslide occurred, prompting a large volume of rock to slide downhill and pile up on the bench at 442 m elevation.

Comments from Referee 2:

P.7 L.17, Please be clear about what is the cumulative force increase, the rate of the increase (including the observed time span). Which criteria were used for the warning, the cumulative force or the rate, or both?

Author's response:

Thanks so much for your careful review. Regarding the monitoring results, it is not written clearly, and a detailed explanation has been made in the manuscript.

The cumulative force increase is the difference between the anchorage force at current time and that at the time the monitoring system is firstly installed.

Regarding the criteria, the criteria are summarized based on a large number of practical applications in rock slopes, and are not strictly quantitative. In fact, the gradual and quick slidings in rock slopes are still very difficult to distinguish. In this study, the cumulative force is considered as the major index. In case that the range of the cumulative increase of [300, 400] is satisfied, the long term warning can be sent; in case that the range of [500, 700] is satisfied, the medium term warning can be considered; if a sudden decrease of 10 kN is monitored under a high force level, the short term warning can be sent. These are the latest criteria summarized and applied. It should be noted that the warning criteria are not strictly quantitative and based on numerous empirical results. They are applied only in the Nanfen open-pit mine. Besides the cumulative force increase, the current force level, the increase rate (sudden increase or dive) and the observation in the field are also necessary to be considered by the field staff.

Comments from Referee 2:

P.7 L.17, What does the long term and the medium term warning refer to?

Author's response:

In case that the range of the cumulative increase of [300, 400] is satisfied, the long term warning can be sent. After that, the monitoring staff in the field is requested to enhance the monitoring intensity, and the monitoring frequency is augmented to be twice per hour.

In case that the range of [500, 700] is satisfied, the medium term warning can be considered. After that, the large equipments are suggested to be evacuated and the mining activities should be temporarily ceased. The monitoring frequency is 4 times per hour.

In case that a significant dive is observed under a high force level, the short term warning can be sent. All staff in the field must be evacuated and the mining activities must be ceased. The monitoring frequency is 8 times per hour.

Comments from Referee 2:

P.7 L.25, Is the mining activity affecting the stability by induced vibrations? Please explain more.

Author's response:

The mining activity usually plays an important role to affect the stability, especially the blasting mining. However, the blasting areas were located on the bottom of the mining camp, and there was a distance of about 500m in between (as shown in Fig. 1). The influence of the vibration on the studied slope was very small. The mining excavation was once partially restarted on October 28, and the anchorage force remained constant. However, it quickly increased during the intensive rainfall on October 30, and the rockslide occurred just one day later. The rainfall was thus considered as the major cause.

Comments from Referee 2:

P.8 L.12, Is the increase of the force starting from 2011-10-02 and on related to rainfall or other causes? please comment. Doesn't the anchorage fail after the rockslide? Why does it keep measuring force?

Author's response:

Thanks for your careful review. The rockslide in 2011 had been discussed in the paper [6]. The excavation on the toe of the slope, from October 2 to 6, 2011, was considered as the major cause. The blasting areas were located on the bottom of the mining camp, and there was a distance of about 500m in between. The influence of the vibration on the studied slope was very small. The excavation at bench 430 was performed 15 days after the last blasting, and on rockslide occurred during the blasting and before the excavation. In addition, there was not rainfall from October 1 to October 5 as shown in Fig. 7c. The rainfall on September 29, 2011 was slight and no influence on the anchorage force was observed; the rainfall on October 6, 2011 was moderate and lasted only 3 hours, it could be a factor of the instability to some extent, but was not the major cause.

After the rockslide, the CRLD cable didn't completely fail, due to its tolerance of large deformation. As shown in Fig. 5a, a relative sliding between the cone and the pipe makes the tolerance possible. As long as the pipe is well anchored in the rock mass, and the rockslide is not too drastic to exceed the tolerance, the CRLD cable can keep working.

Comments from Referee 2:

P.9 L.1, Not very clear what is meant here. I understand that this is the case that the anchorage works and stabilizes the rock mass but what is the point of this phrase?

Author's response:

Thanks so much for your attentive review and kindly reminder, these sentences are not very clear. In some cases, the sliding force is significantly changing during the instability process, but the displacement on the surface of the slope is not yet clearly observed (for example, the potential sliding surface is deep). In these cases, the monitoring system based on the anchorage force of the CRLD cable may be a more suitable tool. "Measurement on the slope cannot work", for example, the GPS surface displacement monitoring point destroyed by rockfall in Fig. 6. This sentences have been rephrased in the manuscript.

Author's changes in manuscript:

In some cases, the sliding force is significantly changing during the instability process, but the displacement on the surface of the slope cannot yet be clearly observed (for example, the potential sliding surface is deep). In these cases, the monitoring system based on the anchorage force of the CRLD cable may be a more suitable tool.

Comments from Referee 2:

P.21 L.21, The authors do not comment at all the role of rock bridges that progressively fail, before leading to the rockslide. This is neither taken into consideration by the numerical model, although very common in rock slides.

Author's response:

Thanks very much for your question, and you are reasonable. The stability of the engineering rock mass is generally determined by the rock blocks and the geological discontinuities. The instability of rock slopes usually proceeds with the breakage of intact rock bridges, and then the global sliding. A consideration of the discontinuous phenomenon into the FEMLIP method is interesting, and this is effectively an ongoing work. We are trying to implementing level-set functions to describe it, but now the FEMLIP method cannot yet solve this issue. In conclusion, this issue will be presented as a shortcoming and a perspective of this study.

According to the geological data, the failure occurs principally along the two-mica quartz schist, which is highly fragmented presenting as blocks and debris and filled with mud. Hence, we considered it as granular material, and simulated it as continuous medium. In addition, based on the mechanical parameters of the rock bridges and the fissures, their weighted average values can be used as the mechanical parameters of the weak zone [4, 5]. In this work, the involved mechanical parameters are reduced in line with the empirical strength reduction method.

Author's changes in manuscript:

In addition, the instability of rock slopes usually proceeds with the breakage of intact rock bridges. The description of this discontinuous phenomenon using the FEMLIP method is worth being considered. By implementing the level-set functions, widely used in X-FEM, the FEMLIP method can be extended to solve the issues of discontinuous media.

[1] He MC, Gong WL, Wang J, Qi P, Tao ZG, Du S, Peng YY (2014) Development of a novel energy-absorbing bolt with extraordinarily large elongation and constant resistance. INT J ROCK MECH MIN 67(67): 29-42

[2] Li, Z.H., Dufour, F., and Darve, F.: Hydro-elasto-plastic modelling with a solid/fluid transition, Computers and Geotechnics, 75, 69-79, 2016.

[3] Li, Z.H., Dufour, F., and Darve, F.: Modelling rainfall-induced mudflows using FEMLIP and a unified hydro-elasto-plastic model with solid-fluid transition, European Journal of Environmental and Civil Engineering, 22(4), 491-521, 2018.

[4] STIMPSON B. Failure of slope containing discontinuous planar joints. *Proceedings of the 19th U.S. Symposium on Rock Mechanics: Stateline Nevada Publication*， 1978, 296–300.

[5] Xia CC, Xu CB. Study of Fracturing algorithm of intermittent joint by DDA and experimental validation. *Chinese Journal of Rock Mechanics and Engineering,* 2010, 29(10): 2027-2033.

[6] Li, Z.H., Jiang, Y.J., Tao, Z.G., He, M.C.: Monitoring prediction of a rockslide in an open-pit mine and numerical analysis using a material instability criterion, Bulletin of Engineering Geology and Environment, published online, 2018b.

Short comments:

Received and published: 2 May 2018

Short comments from Mubashir Aziz:

The monitoring method is interesting, and the comparison between the monitoring data and the numerical result, the global second order work, is a good attempt. I just wonder how the CRLD cable is installed in the borehole, how it is anchored?

Author's response:

Thanks for your kindly comments. Regarding the installation of the CRLD, the borehole is drilled through the geological discontinuity as shown in the figure as follows. The sleeve pipe is anchored in the borehole by the grouting material generally with a thickness of 14.5 mm, and one end of the stands is fixed on the slope surface.

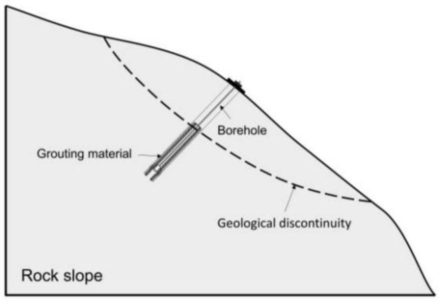

Short comments from Mubashir Aziz:

In addition, the space is missed in P.20, L.11 and L.20 (However, the mining activity. . ., . . .prove that the October 31, 2016 rockslide. . .).

Author's response:

Thanks for your kindly comments, the errors will be corrected in the manuscript.

Short comments from Mubashir Aziz:

Finally, the authors claim that the global second order work could be used as a safety factor. It's a little abrupt. It is better to compare it with a current one, for example, the safety factor used in the FLAC3D software.

Author's response:

Thanks for your kindly comments. Regarding the safety factor, the second order work can describe the stability of the structure in the Lyapunov sense, and not only a limit equilibrium state. It is thus more general and more physical. In addition, the safety factor used in the FLAC3D software cannot solve the large strain problems, but it is not an obstacle for the second order work. Thanks for your valuable suggestion, more detailed discussion about the safety factor will be given in the manuscript.

Real-time monitoring and FEMLIP simulation of a rainfall-induced rockslide

ZhaoHua Li[1], ZaoGang Tao[1], YuanJun Jiang[2*], Qian Lv[1], Felix Darve[3], ManChao He[1]

1. State Key Laboratory for Geomechanics and Deep Underground Engineering, China University of Mining and Technology, Beijing, 100083, China
2. Institute of Mountain Hazards & Environment, Chinese Academy of Sciences, Chengdu, China
3. Grenoble CNRS, UMR 5521, 3SR, Grenoble Alpes University, Grenoble, France

Abstract. Rockslides are a common and devastating problem affecting mining and other engineering activities all over the world; consequently, there have been many studies into their prediction and prevention. This study focused on a recent rockslide in an open pit mine in Liaoning province, China. The stability of the rock slope under excavation and rainfall conditions were monitored using an efficient real-time monitoring system. A further numerical analysis was performed using the Finite Element Method with Lagrangian Integration Points (FEMLIP), and two forms of the normalized global second order work were calculated to analyze the stability of the rock slope. In fact for the future it would be very interesting to compare in real time measurements and simulations, and not only to develop back computations after failure. The numerical results indicate that the rock slope remained stable during excavation, yet lost stability after subsequent rainfall. Water infiltration, along with a major geological discontinuity, degraded the strength of the weak zone and induced the rockslide. The monitoring approach presented its robustness and generality, and was worth being generalized. The numerical approach proposed the evolution of the safety factor, comparing the monitoring data, and the mechanism of the rockslide was determined. It could be used as an assistant tool for the disaster predictions.

Keywords: rockslide, second order work, FEMLIP, prediction, landslide monitoring, rainfall.

Acknowledgements

First, the authors sincerely acknowledge the CAS Pioneer Hundred Talents Program for making possible the completion of this research. The research presented in this paper was also jointly supported by the National Natural Science Foundation of China (Grant No. 41502334) and fund of the Institute of Mountain Hazards and Environment (Grant No. SDS-135-1705 and Grant No. SDS-135-1704). The authors wish to acknowledge these financial contributions and convey our appreciation to these organizations for supporting this basic research.

[*] Corresponding author: Yuanjun Jiang, Associated research fellow, PhD, E-mail: yuanjun.jiang.civil@gmail.com. Institute of Mountain Hazards & Environment, Chinese Academy of Sciences, 9, Block 4, Renminnanlu Road, Chengdu, 610041, China. TEL: 8628-85228816, Fax: +8628-85222258

1 Introduction

Rockslides characterized by sudden occurrence, large volume, and frequently high acceleration are a hazard around the world. The mechanisms driving this hazard are complex, and rockslides can be influenced by a large number of factors, including topography, earthquakes, human factors, and climatic variation (Chen et al., 2006; Wang et al., 2011; Tu et al., 2009). Rockslides can occur suddenly and rapidly; for example, after rock slopes undergo a series of slow and imperceptible changes. For civil safety and engineering activities, careful monitoring and accurate predictions are a challenging geological and geotechnical issue.

Not all rock slope instabilities induce catastrophic consequences. Recently, a sudden rockslide in an open-pit iron ore mine was successfully monitored on October 31, 2016. Early warnings were received, and fatalities and economic damage were avoided. This rockslide occurred after excavation on the toe of slope and subsequent rainfall lasting about 21 hours. The slope was reinforced and the stability was monitored using the Constant-Resistance-Large-Deformation (CRLD) cable, which could support a large elongation of 2m, and provide a constant resistance during the large elongation (He, 2009; He et al., 2014). Using real-time monitoring data, the early warning system sent urgent sliding warnings, so that all staff and equipment were evacuated in time. After 4 hours, global instability occurred and a rock mass with a volume of 1.35 x 10^4 m^3 slid down slope. It should be noted that this rockslide was the second sliding in the same area, and there was another rockslide, induced by excavation and occurred in 2011. It was also successfully predicted using the monitoring system, and the reliability of this monitoring system for excavation-induced rockslides has been proven (Li et al., 2018b). One of the objectives of this study is to present the monitoring of the second rockslide in 2016, and to discuss the adaptability of the monitoring system for rockslides induced by different triggering factors. Fig. 1 illustrates the remote-sensing system for monitoring and predicting landslides. The CRDL cables are usually installed in the rock mass with an inclination of 25^o, and their fixed parts are anchored under the weak zone. The sensing device is installed at the point D1, as shown in Fig. 1a, and the monitored data are sensed by the receiver in the Beidou satellite and then transmitted to the indoor monitoring center. By means of the satellite system, the monitored anchorage force can be transmitted once per 1-2 h, in real mining projects (Li et al., 2018b).

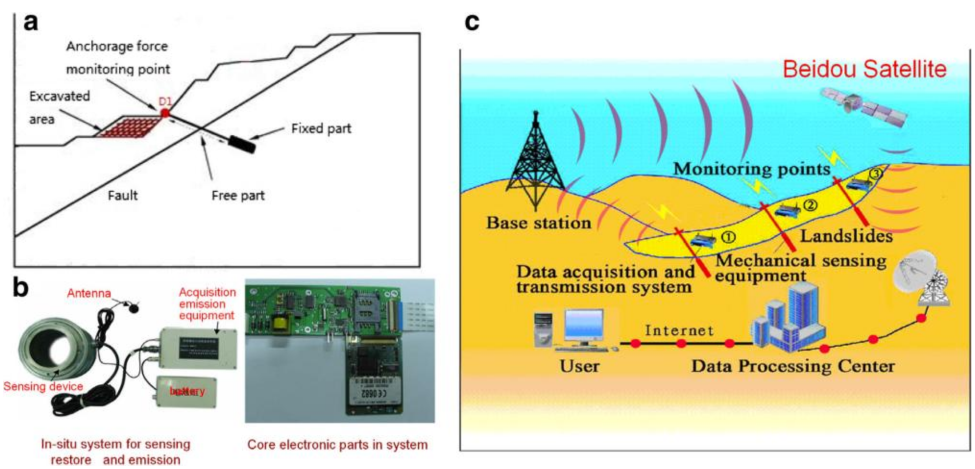

Figure. 1 Remote-sensing system for monitoring and predicting landslides: (a) simplified model of the CRLD cable sliding-resistant system; (b) remote-sensing equipments, and (c) Beidou satellite remote sensing system for monitoring the anchorage force (Li et al., 2018b).

The numerical method is an important tool to analyze the failure mechanisms and the instability issues of geomaterials. Besides the classical Finite Element Methods (FEM) and the Finite Difference Method (FDM), diverse new numerical approaches have been proposed (Soga et al., 2016). Smooth particle hydrodynamics (SPH) (Cascini et al., 2014) has been used to simulate channelized landslides of flow type; the material point method (MPM) (Soga et al., 2016; Abe et al., 2013; Marcelo et al., 2016; Bandara et al., 2016) can describe the whole process of landslide movement using hydro-mechanical coupling; the discrete element method (DEM) has been used to model the instability of jointed rock slopes (Dong et al., 2015; Huang et al., 2015); and the Finite Element Method with Lagrangian Integration Points (FEMLIP) method (Cuomo et al., 2013) is developed from the particle-in-cell method (PIC) (Harlow 1964; Moresi et al., 2002; Moresi et al., 2003) and satisfies the two requirements for simulating the complete evolution of landslides: precise tracking of internal variables and the ability to solve large displacements (Li et al., 2016; Li et al., 2018a; Prime et al., 2013). In contrast to the material point method, the numerical weight of material particles used in the FEMLIP method is updated at each time step, leading to an acceptable calculation cost, owing to the use of an implicit solver (Li et al., 2018a). Each method has its advantages and drawbacks, and the details can be referred to the previous contributions (Soga et al., 2016; Li et al., 2018a). In the study, the FEMLIP method was used to simulate the rockslide, because it overcame the problem of mesh distorsion during the large deformation of geomaterials, and could easily take into account the normalized global second order work as a safety factor.

This paper is organized as follows: section 2 presents the engineering geological properties, and the monitoring anchorage force corresponding to the studied rockslide. Section 3 describes our FEMLIP model of the studied rockslide. First, the hydro-elasto-plastic model is briefly presented; second, FEMLIP modeling of the rockslide is performed; third, the numerical results are analyzed and compared with monitoring data, and the cause of the rockslide is determined. In Section 4, some conclusions and future research prospects are discussed.

2 Engineering geological properties and real-time monitoring data

2.1 Location of study site

The Nanfen open-pit iron mine is one of the largest iron ore mines in Asia, with a mining history of more than 100 years. This mine is situated in Nanfen city, Liaoning province, China. In recent years, the local slope has reached 552 m (elevation 142 to 694 m, and the bottom elevation of the mining was 160 m in 2011 (Li et al., 2018b) owing to mining of shallow strata and an increase in mining depth. From 1999 to 2016, several rockslides of different scales were reported, due to both mining activity and rainfall. This study focused on a rockslide on October 31, 2016, which followed excavations on the toe of slope and occurred after a period of rainfall. As shown in Fig. 2a, several CRLD cables were installed within the area of an old landslide, to reinforce the slope and monitor the anchorage force, and the studied rockslide at elevations between 442 and 502 m (red zone in Fig. 2a) was monitored by the CRLD cable with a number of 478-3. In the same area, a previous rockslide occurred in 2011 at elevations between 442 and 550 m (purple zone in Fig. 2a), and it was monitored using the CRLD cable with a number of 478-3' (green point in Fig. 2a).

2.2 Engineering geological properties

The open-pit mine is located at southern side of the Heibeishan inverted anticline, composed of the archean Anshan group, proterozoic Liaohe group, sinian and quaternary strata. Fig. 2b shows that the rockslide occurred on the heading wall, an inclined hard rock slope consisting of chlorite schist and chlorite-hornblende separated by a major weak zone with a slope of 48°; and a strike angle of 295°. The hanging wall is an anti-inclined rock slope consisting principally of migmatitic gneiss and two-mica quartz schist with a hardness of 13–16, and a slope of 46°–48°. The weak zone consisted of the strongly fragmented two-mica quartz schist, with a thickness of about 2m and a length of about 600m (Li et al., 2018b). This weak zone was considered to run through the heading wall, and controlled the stability of the slope on the heading wall. It partially emerged after the rockslide, and was humid and partially sandwiched with mud.

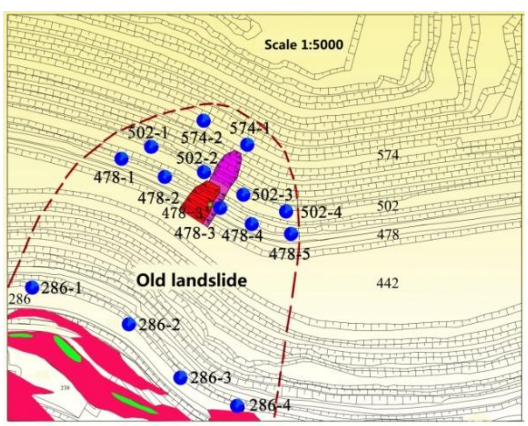

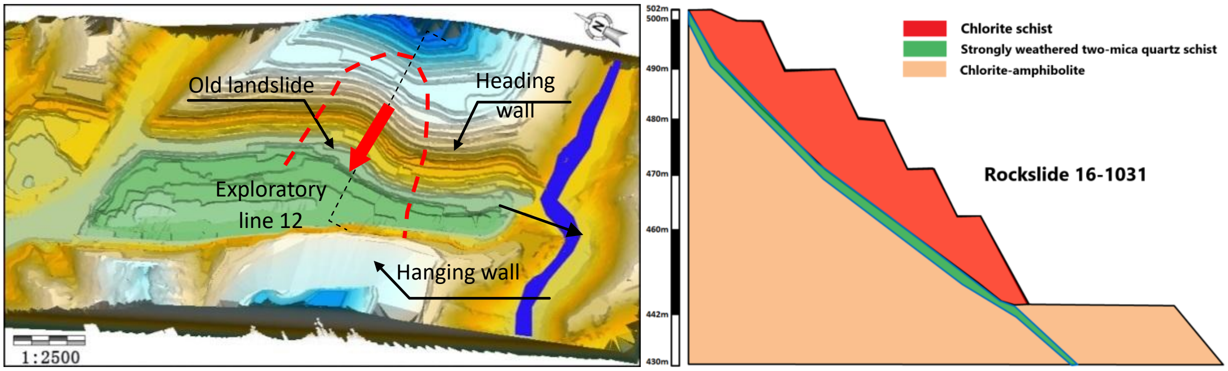

Figure 2. (a) Plan graph of the Nanfen open-pit iron mine rockslide location. The red area shows the location of the studied landslide that occurred on October 31, 2016. The purple zone shows the boundary of a rockslide that occurred in 2011. Blue circles show the current distribution of force monitoring points, and the green one with a number 478-3' indicates the CRLD cable served during the rockslide in 2011; (b) Relief map of the Nanfen mine; (c) geological profile along exploratory line 12

2.3 Site survey and rockslide characteristics

In order to understand in detail the geological properties of the open-pit mine, detailed investigations were performed along 28 exploratory lines. For each exploratory line, 140 boreholes were drilled at intervals of 50 m. The dip direction of the studied rockslide was close to the direction of the exploratory line 12 (see Fig. 2b); the length along the dip direction was 60 m. The width along the strike line was 50 m, and the corresponding surface was about 3000 m^2. The rockslide was inclined and had a volume of $1.35 \times 10^4\ m^3$; the maximum thickness of the sliding bodies was about 18 m.

The landslide front was situated on a bench at 442 m elevation, and deposits were concentrated at this level and on the slope between the benches at 442 and 430 m elevation. The trailing edge of the rockslide was situated on the bench at 502 m elevation, where a sinking of 7.5m was induced by the rockslide, as shown in Fig. 3.

Figure 3. Sinking observed on the top of the slope

Figure 4. Slip surface consisting of strongly fragmented two-mica quartz schist

The slip surface mainly included a major geological discontinuity, and was smooth and significantly striated (Fig. 4). The major geological discontinuity, which consisted of strongly fragmented two mica-quartz schist, decreased in strength owing to water infiltration. After the rockslide, rock along the slip surface was moist and the mechanical properties were observed to be significantly degraded. Throughout the rockslide, the slide body did not completely disintegrate, but slid as big blocks along the slip surface.

2.4 Real-time monitoring

The rock slope was under real-time monitoring by the CRLD cables, developed in the State Key Laboratory for Geomechanics and Deep Underground Engineering. The cable of this type can support large deformation (up to 2 m) while offering constant resistance. The development of the CRLD cable not only reinforced the anchoring ability, but also made it possible to monitor crustal stress in deep strata, and it has successfully predicted the rockslide occurred in 2011, due to the excavation on the toe of the slope (Li et al., 2018b). As shown in Fig. 5 (a), the CRLD cable is composed of a piston-like cone body installed on a bundle of cables (6-8 cables), a sleeve pipe with an inner diameter slightly smaller than the diameter of the large-end of the cone; a face pallet served as the retention elements. The anchored end is fixed using grout, and the relative displacement appears between the sleeve pipe and the cables when an axial pull load larger than the constant resistance of the cable is exerted on the face pallet end. The large-end diameter of the cone is slightly larger than the inner diameter of the sleeve pipe, in order to produce sufficient frictional resistance during the relative movement, and to avoid failure of the sleeve pipe. Fig. 5 (b) shows the constant resistance and large deformation properties according to the static pullout tests in laboratory, and this advantage makes the monitoring and prediction possible, during occurrence of landslides, even if the significant relative movement appears on the sliding surface. More details of the CRLD cable and the remote monitoring system can be found in the previous contributions (He, 2009; Sun et al., 2011; He et al., 2014).

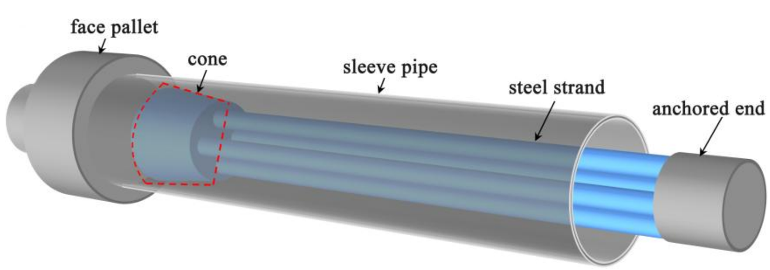

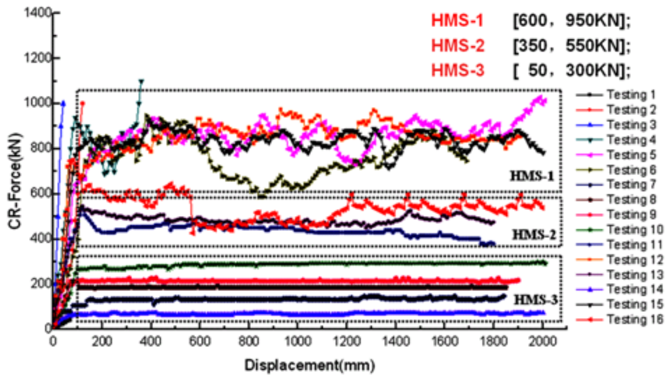

Figure 5. (a) Structure of the CRLD cable in three-dimensional view (Li et al., 2018b); (b) constant resistance and large deformation exhibited by the CRLD cable of different specifications, under static loading.

In the old landslide area (as shown in Fig. 1), 15 anchorage force monitoring points and two GPS surface displacement monitoring points were installed. One of the surface displacement monitoring points was located on the bench at 478 m, within the domain of the studied rockslide, and it was destroyed by a rockfall during the rockslide (Fig. 6). In the hanging wall, which was stable compared with the footwall, one GPRS relay station and one Beidou satellite relay station were installed. These installations were completed in August 2010 and became operational in October 2010, and have proposed several successful predictions for rockslides occurred in this zone, including the one in 2011 (Li et al., 2018b).

Figure 6. GPS surface displacement monitoring point destroyed by rockfall

2.5 Anchorage force monitoring

From September 7, 2015, the anchorage force monitored at point 478-3 showed a series of slow increases and three sudden increases, which accumulated a force increase from 270kN to 600kN until September 1, 2016, as remarked by the points A, B and C in Fig. 7a. Before September 1, 2016, the cumulative value had not strictly reached the warning threshold proposed by He (2009), and no obvious fissures were observed according to in-situ surveys; therefore, no warning was sent. As a result of constant mining activity, the cumulative increase of anchorage force reached 330 kN and the fourth sudden increase appeared after September 1, 2016, as remarked by the point D in Fig. 7a. Although no fissures were observed, the first long-term warning was sent due to the sudden increase by the field staff, and the monitoring frequency was increased to twice per hour. When the anchorage force returned to constant on October 1, 2016, the cumulative force increase exceeded 220 kN and a few surface fissures appeared, the medium term warning was sent. The mining activities were ceased and the monitoring frequency was doubled to 4 times per hour. In the following days, the curve remained constant and no obvious fissures continued to develop; therefore, mining excavations restarted along the bench at 442 m elevation on October 28, 2016. On October 30, the anchorage force suddenly increased again at 04:53, and reached a peak value of 855 kN at 17:07, during a period of rainfall. A subsequent dive of the anchorage force was observed. The short term warning was sent at 08:56 on October 31, and all staff was urgently evacuated. At 23:52 on October 31, the rockslide occurred, prompting a large volume of rock to slide downhill and pile up on the bench at 442 m elevation.

Mining activities on the toe of the rock slope explain the first 4 sudden increases in monitored anchorage force. However, the last excavation before the rockslide occurred on October 28, 2016, and there was no obvious increase in the curve of anchorage force (Fig. 7b), though it remained a high level. On October 30, 2016, the last abrupt increase in anchorage force appeared during a period of intense rainfall, before the subsequent rockslide on October 31, 2016. Based on the survey data, this rainfall was considered to directly trigger this rockslide.

Fig. 7 (c) shows the monitoring anchorage force during the excavation-induced rockslide in 2011, and the similar evolution, that the anchorage force quickly increases to a peak and sharply decreases until the rockslide occurs, is observed. Comparing Figs. 7 (a) and (b), both of the peak and the decrease during the rockslide are in a significantly larger scale, with values of 1678 kN and about 200 kN, respectively. The reason was that the CRLD cable 478-3' was located within the range of the rockslide 2011, and thus completely reflected the variation of the sliding force; the CRLD cable 478-3 was located outside the range of the rockslide 2016, so the variation of the sliding force was partially reflected. However, it does not obstruct the successful monitoring and prediction.

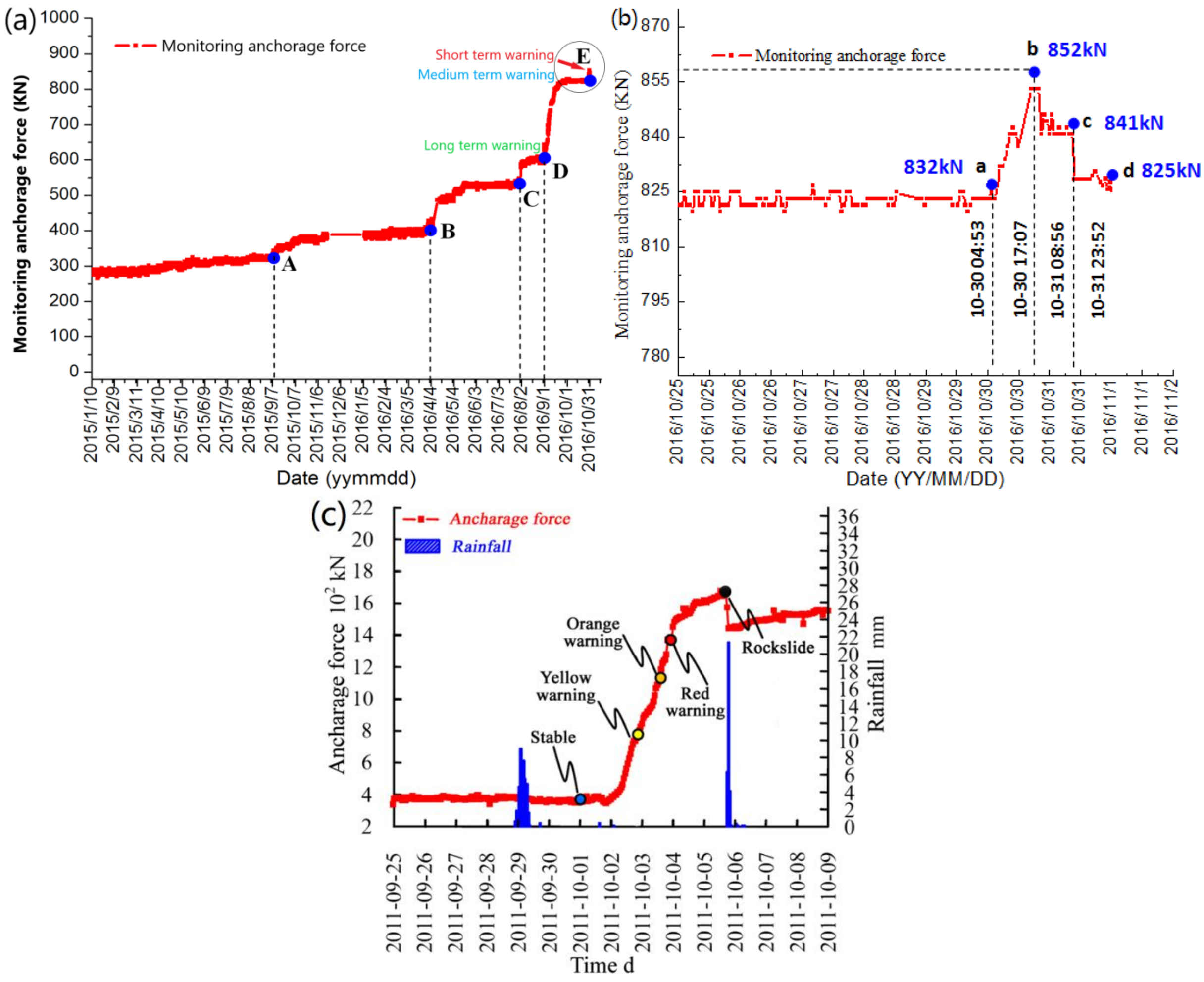

Figure 7. Real-time monitoring curve of the anchorage force. (a) points A–E represent five sudden increases before the rockslide in 2016; (b) anchorage force during the rockslide in 2016 (partially enlarged from part a); (c) monitoring anchorage force during the rockslide in 2011 (Li et al., 2018b).

The prediction of geological disasters is a complex issue, with rainfall, earthquakes, and human activities all presenting potential triggers. Variables such as stress, strain, and water pressure are often used for monitoring purposes; however, for landslides, these variables are not always predictive. Anchorage force monitoring was chosen because it can accurately reflect increasing sliding force and the degradation of the mechanical properties of geomaterials, which in turn result in increased anchorage force and the possibility of slope instability. In some cases, the sliding force is significantly changing during the instability process, but the displacement on the surface of the slope cannot yet be clearly observed (for example, the potential sliding surface is deep). In these cases, the monitoring system based on the anchorage force of the CRLD cable may be a more suitable tool.

3 Numerical analysis using FEMLIP

Different instability mechanisms complicate the analysis of rockslides, and many issues remain open to discussion. Although the stability of rock slopes hinges on a large number of factors, such as the type and the history of the rock, the size of the slope and so on, the geological discontinuities, which have lower strength and more commonly developed fissures, also play an important role in the mechanical behavior and the stability, especially for the geological discontinuity controlled slopes (Regmi et al., 2012; Zhang et al., 2016). Generally, geological discontinuities have higher porosity and function as channel systems for water infiltration (Regmi et al., 2012). The rock slope in the study area is characterized by a major geological discontinuity of highly fragmented two-mica quartz schist. The two-mica quartz schist is highly fragmented presenting as blocks and debris, and filled with mud, and can be considered as granular material.

We used the FEMLIP method to realize the large deformation during the rockslide. By using the FEMLIP method, the simulated materials are discretized by an Eulerian mesh and a series of Lagrangian material points, the control equations are solved and the solution is obtained in the Eulerian calculation mesh. After interpolation according to corresponding shape functions, the internal variables (stress, strain, water content, etc.) can be obtained for each material point. At each time step, the position of material points is refreshed. In this process, the material points move in line with the deformation of the studied material, but the mesh is not deformed. The relative movement between the material points and the mesh makes the simulation of large deformation possible (Li et al., 2018c).

3.1 Elasto-plastic model incorporating complete hydro-mechanical coupling

In this study, an elasto-plastic model, the PLASOL model, was used to describe the elasto-plastic behavior with plastic hardening for the major discontinuity, according to experimental data (as shown in Figs. 9). For describing the decrease of strength on the major geological discontinuity due to wetting, a Bishop's type effective stress formulation and modified Van Genuchten water retention curves (WRCs) were introduced into the PLASOL model.

3.1.1 PLASOL model

This non-associated elasto-plastic model was first used for solving structural geology problems within the framework of finite element methods (Barnichon, 1998), and is also appropriate for dealing with a wide range of geomaterials (Lignon et al., 2009; Prime et al., 2013; Prunier et al., 2016; Li et al., 2016; Li et al., 2018b). A Van Eekelen plasticity criterion (Van Eekelen, 1980), which is similar to the Mohr-Coulomb criterion but avoids geometric singularities, is used as the plastic limit in the model. Let us invoke three effective stress tensor invariants $J_{1\sigma'} = \mathrm{tr}(\boldsymbol{\sigma'})$, $J_{2\sigma} = \sqrt{\mathrm{tr}(\boldsymbol{\tau}^2)}$, $J_{3\sigma} = \sqrt[3]{\mathrm{tr}(\boldsymbol{\tau}^3)}$, $(\boldsymbol{\tau} = \boldsymbol{\sigma}' - \frac{1}{3}\mathrm{tr}(\boldsymbol{\sigma'})\boldsymbol{I})$, where $\boldsymbol{\sigma}'$ is the Bishop's effective stress, calculated as follows:

$$\boldsymbol{\sigma}' = \boldsymbol{\sigma} - u_a\boldsymbol{m} + \chi(u_a - u_w)\boldsymbol{m} \tag{1}$$

where $\boldsymbol{\sigma}$, u_a, and u_w are the total stress vector, the isotropic air pressure, and the isotropic water pressure, respectively; χ is the Bishop's parameter taken as a scalar in this model; and $\boldsymbol{m^T} = (1,1,1,0,0,0)$, $s = u_a - u_w$ is the suction value. For the sake of simplification, the Bishop's proposition (Bishop, 1959) was used to formulate parameter χ in this study:

$$\chi = Sr \tag{2}$$

Considering the Bishop's effective stress, the expression of the Van Eekelen yield criterion can be written as follows:

$$f = J_{2\sigma} + m\left(J_{1\sigma'} - \frac{3c}{\tan\varphi_c}\right) = 0 \tag{3}$$

where c is cohesion, φ_c is the mobilized friction angle under triaxial compression conditions, and m is a coefficient defined as follows:

$$m = a\left(1 + b\sin(3\beta)\right)^n \tag{4}$$

The Lode angle β is given by $\cos 3\beta = \sqrt{6}\left(\frac{J_{3\sigma}}{J_{2\sigma}}\right)^3$, parameters a and b are functions of the friction angles φ_c (compression path) and φ_e (extension path), as defined by:

$$a = \frac{r_c}{(1+b)^n}, \qquad b = \frac{\left(\frac{r_c}{r_e}\right)^{\frac{1}{n}} - 1}{\left(\frac{r_c}{r_e}\right)^{\frac{1}{n}} + 1} \tag{5}$$

where parameters r_c and r_e are the reduced radii for triaxial compression and extension tests, respectively, and are calculated as follows:

$$r_c = \frac{1}{\sqrt{3}}\left(\frac{2-\sin\varphi_c}{3-\sin\varphi_c}\right), \qquad r_e = \frac{1}{\sqrt{3}}\left(\frac{2\sin\varphi_e}{3+\sin\varphi_e}\right) \tag{6}$$

The exponent n controls the shape of the yield surface, and the default value is -0.299 according to the work of Van Eekelen (1980).

In the PLASOL constitutive model, the plastic hardening of the yield surface during loading is controlled by internal variables (the cohesions and friction angles), which are functions of theVon Mises equivalent plastic strain: $\boldsymbol{\varepsilon}_{eq}^p = \sqrt{\frac{2}{3} e_{ij}^p e_{ij}^p}$, ($\boldsymbol{e}^p = \boldsymbol{\varepsilon}^p - \frac{1}{3}\mathrm{tr}(\boldsymbol{\varepsilon}^p)\boldsymbol{I}$. Consequently, the compression, extension friction angles, and cohesion formulated in Equations (7), vary between elastic initial values (c_0, φ_{e0}, φ_{c0}) and plastic limit values (c_f, φ_{ef}, φ_{cf}), depending on the equivalent plastic strain $\boldsymbol{\varepsilon}_{eq}^p$ and the hardening parameters B_c and B_p (Lignon et al., 2009; Prunier et al., 2009).

$$\begin{gathered}
\varphi_c = \varphi_{c0} + \frac{(\varphi_{cf} - \varphi_{c0})\boldsymbol{E}_{eq}^{p}}{B_p + \boldsymbol{E}_{eq}^p} \\
\varphi_e = \varphi_{e0} + \frac{(\varphi_{ef} - \varphi_{e0})\boldsymbol{E}_{eq}^{p}}{B_p + \boldsymbol{E}_{eq}^p} \\
c = c_0 + \frac{(c_f - c_0)\boldsymbol{E}_{eq}^{p}}{B_c + \boldsymbol{E}_{eq}^p}
\end{gathered} \tag{7}$$

Furthermore, the dilatation angle ψ is required to define the non-associated plastic law (Prunier et al., 2009; Li et al., 2016). In total, 13 parameters are required to adequately describe the elasto-plastic behavior of geomaterials:

E, v: Young's modulus and Poisson's coefficient, respectively
φ_{c0}, φ_{cf}: mobilized friction angles at elastic and plastic limits under triaxial compression, respectively
φ_{e0}, φ_{ef}: mobilized friction angles at elastic and plastic limits under triaxial extension, respectively
ψ_c, ψ_e: dilatation angles under triaxial compression and extension, respectively
c_0, c_f: cohesion at elastic and plastic limits, respectively
B_c, B_p: hardening parameters
n: exponent controlling yield surface shape

3.1.2 Water retention curves

In order to determine the Bishop's parameter χ from the degree of saturation, it is necessary to determine the relationship between suction and the degree of saturation. A large number of water retention models have been proposed (Van Genuchten, 1980; Parlange, 1980; James et al., 1998; Feng and Fredlund, 1999), and the modified

Van Genuchten model (Van Genuchten, 1980; James et al., 1998) was selected to complete the hydro-mechanical coupling in this study because the boundary curves are simple and commonly used. The formulation of this model is as follows:

$$Sr_v = Sr_{res} + (Sr_{sat} - Sr_{res})\left(1 + \left(\frac{a_v s}{P_{atm}}\right)^{n_v}\right)^{\frac{1}{n_v}-1} \tag{8}$$

where index v stands for d or w in the drying or wetting processes, respectively; Sr_{res}, Sr_{sat}, and Sr_v are the residual, saturated, and current degrees of saturation, respectively; and a_v and n_v are two parameters depending on porosity, whose expressions can be found in (Arairo et al., 2013).

3.1.3 Second order work criterion

In this study, instead of classical plasticity criteria, the second order work criterion was used, and the sign of the second order work indicated local and global failures.

As the lower border of the bifurcation domain and the most conservative failure criterion, the second order work criterion has been systematically investigated for evaluating the stability and failure of geomaterials(soils and jointed rocks) (Darve and Servant, 2004; Darve et al., 2004; Laouafa et al., 2011; Duriez et al., 2011; Nicot et al., 2011) . The local second order work and its normalized form are written as follows:

$$d^2w = d\sigma_{ij}^{'}\, d\varepsilon_{ij} \tag{9a}$$

$$d^2w_{norm} = \frac{d^2w^i}{\|d\boldsymbol{\sigma}'^{\boldsymbol{i}}\|\|d\boldsymbol{\varepsilon}^{\boldsymbol{i}}\|} = cos\alpha^i \tag{9b}$$

where d^2w_{norm} is the normalized local second order work at material point *i*, and $\|d\boldsymbol{\sigma}'^{\boldsymbol{i}}\|$ and $\|d\boldsymbol{\varepsilon}^{\boldsymbol{i}}\|$are the norms of the stress increment and the strain increment of the material point *i*, respectively. Hence, the d^2w_{norm} is equal to the cosine of the angle α between the incremental stress and strain vectors, and its value is thus limited between -1 and 1.If $d^2w_{norm} > 0$ for all loading directions, the material is strictly stable; if $d^2w_{norm} < 0$ at least in one loading direction, the material is considered potentially unstable; and if $d^2w_{norm} < 0$ in the current loading direction, the material is unstable, and diffuse or localized failures can occur. In order to save computational time in the simulation, the local second-order work (see equations 9) was only calculated for the current loading direction.

In order to analyze the global instability for the boundary value problems, an appropriate expression of normalized global second order work is needed. According to the integral expression of d^2w (Hill, 1958): $D^2W = \int_V d\boldsymbol{\sigma}' d\boldsymbol{\varepsilon} dV = d\boldsymbol{Q}^{\boldsymbol{t}} d\boldsymbol{F}$, with V the volume of interest, $d\boldsymbol{Q}$ and $d\boldsymbol{F}$ the global nodal incremental displacement and force, respectively, the normalized global second order work was firstly proposed as follows (Khoa et al., 2006):

$$D^2W_{norm} = \frac{D^2W}{\|d\boldsymbol{Q}\|\|d\boldsymbol{F}\|} = \frac{d\boldsymbol{Q}^{\boldsymbol{t}} d\boldsymbol{F}}{\|d\boldsymbol{Q}\|\|d\boldsymbol{F}\|} = \frac{\sum(d^2w^i \cdot \omega^i J^i)}{(\sum \omega^i J^i)(\sum \|d\boldsymbol{\sigma}'^{\boldsymbol{i}}\|\|d\boldsymbol{\varepsilon}^{\boldsymbol{i}}\|)} \tag{10}$$

where ω^i is the numerical weight of the material point *i*, and J^i is the determinant of the Jacobian matrix. This expression is convenient to compute, but it is mesh dependent (Prunier et al., 2009). Recently, a new expression, independent from the number of elements, has been proposed as follows (Prunier et al., 2016):

$$D^2W_{norm} = \frac{D^2W}{\int_V \|d\boldsymbol{\sigma}\|\|d\boldsymbol{\varepsilon}\| dV} = \frac{\sum(d^2w^i \cdot \omega^i J^i)}{\sum(\omega^i J^i \cdot \|d\boldsymbol{\sigma}'^{\boldsymbol{i}}\|\|d\boldsymbol{\varepsilon}^{\boldsymbol{i}}\|)} \tag{11}$$

Evidently, both the numerators in equations 10 and 11 are identical, but the denominator in equation 10 is larger with finer mesh, and that in equation 11 is mesh independent. Noted that equation 11 needs the use of a sufficiently open numerical code, in order to manipulate basic integration operators over the elements or to get access to shape functions and mesh description.

3.2 Numerical analysis of the Nanfen rockslide

3.2.1 Geometry and boundary conditions of the rockslide model

Geological data from the field survey and engineering geology drilling showed that the sliding surface was principally along the major geological discontinuity (i.e., along strongly fragmented two-mica quartz schist). The FEMLIP model of the rock slope was established in a calculation domain, in which the horizontal and vertical dimensions were 120 m and 80 m, respectively. The calculation domain was discretized by 1920 meshes, and each mesh consisted of 25 material points. The slope was composed of three materials (Fig. 8): chlorite-hornblende stable bedrock, chlorite schist slide bodies, and a two-mica quartz schist as the major geological discontinuity. The model dimensions were as follows: height 72 m; width 110 m; bedrock height and width 64 and 60 m, respectively; widths of the seven benches were 5, 5, 10, 5, 5, 5, and 30m, respectively.

In this model, all boundaries were free slip, and the horizontal displacement at the left boundary and the vertical displacement at the bottom boundary were constrained. Gravity increased linearly for the first 150 time steps, until a value of 9.81 m/s^2 was reached. For sake of simplification, the initial suction in the major geological discontinuity was assumed homogeneously distributed. Moreover, an excavation on the toe of the slope was performed at the 38th hour, and rainfall on the top surface induced downward water infiltration under a constant water flux of 24 mm/h over 21 hours.

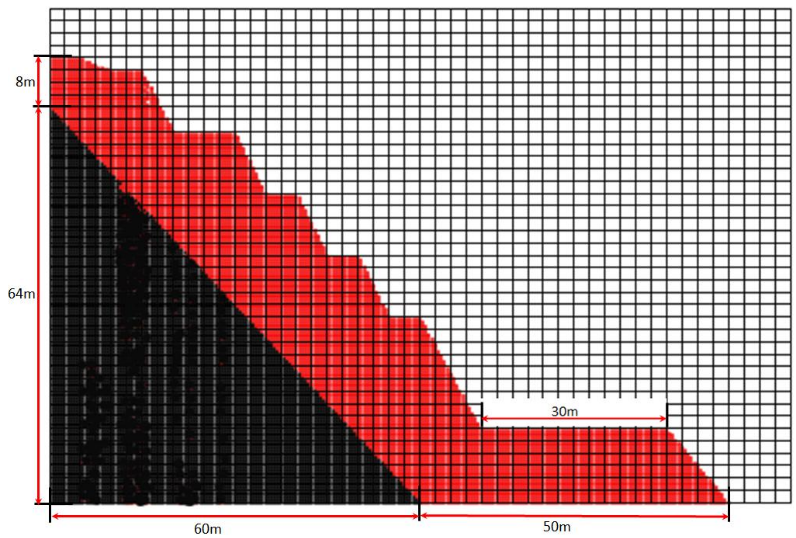

Figure 8. Geometry of the rock slope FEMLIP model. Stable bedrock (black layer) is chlorite-hornblende. The slide body (red) comprises chlorite schist. The interface between the black and red layers comprises a two-mica quartz schist functioning as the major geological discontinuity

3.2.2 Determination of physical parameters

In the model, all three materials were described by elasto-plastic constitutive law, and the hydro-mechanical coupling was taken into account only for the chlorite schist and the highly fragmented two-mica quartz schist. The geomechanical parameters were estimated according to the triaxial compression tests and geological survey. The sample of two mica-quartz schist for the triaxial compression tests are showed in Fig. 9 (a). Figs. 9 (b and c) gave typical stress-strain curves under a confining stress of 20 MPa, for the sample with a degree of saturation of 43% and the one in saturated state, respectively. The values of c_0 and c_f could be thus estimated. It was necessary to reduce the strengths obtained from the experimental data, because the weak zone emerged after the rockslide presented a high discontinuity density. According to the empirical strength reduction method, the cohesions used in the paper were reduced by Equation $c = \frac{c_i}{n+k}$. c and c_i were reduced cohesion and that of intact rock sample, respectively. n was discontinuity density, which was assigned to be 30, and k was a coefficient related to the fragmentation index with a value of 40. Considering the empirical strength reduction method and the values recommended by in-situ tests (Sun et al., 2011; Yang et al., 2012; Li et al., 2018), the elasto-plastic parameters were summarized in Table 1.

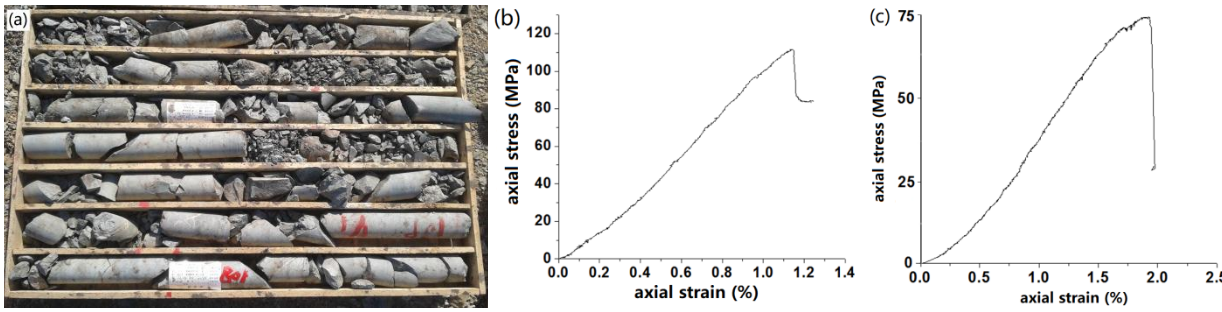

Figure 9. Triaxial compression tests for determining the geomechanical parameters of the two mica-quartz schist. (a) samples for the experimental tests, typical stress-strain relations under confining stress of 20 MPa, for (b) the samples with a degree of saturation of 43%, and (c) the samples in the saturated state respectively.

The degree of saturation of the two-mica quartz schist before rainfall was 43%. The permeability of the two-mica quartz schist was $k_1 = 2 \times 10^{-1}\ \mathrm{cm/s}$ and that of the chlorite schist was $k_2 = 1 \times 10^{-8}\ \mathrm{cm/s}$, according to a top surface aperture of 1 mm and a slope surface aperture of less than 0.025 mm; consequently, the permeabilities were considered strong and very weak, respectively (GB50487-2008). It should be noted that decreasing strength of rocks under rainfall conditions is generally due to the saturation effect in the unsaturated stage and the softening effect in the saturated stage. The latter is generally a long-duration process, and is not the objective of this study. The former results in an increasing degree of saturation and a decreasing suction; thus, the apparent cohesion and strength are reduced according to Equation 12:

$$\boldsymbol{\tau} = c^{'} + \boldsymbol{\sigma}^{'}\tan\varphi^{'} = \left(c^{'} + \chi s\tan\varphi^{'}\right) + \overline{\boldsymbol{\sigma}}\tan\varphi^{'} \tag{12}$$

where c' is the effective cohesion measured from the sample on the top surface after rainfall, and $c = c^{'} + \chi s\tan\varphi'$ is the apparent cohesion measured from the sample before the rockslide. With the assumption of $\chi = Sr$, the suction after rainfall could be considered 0, and the initial suction before rainfall could be obtained by the expression: $c - c^{'} = \chi s\ \tan\varphi^{'} = 23kPa$. The initial suction was thus 105 kPa.

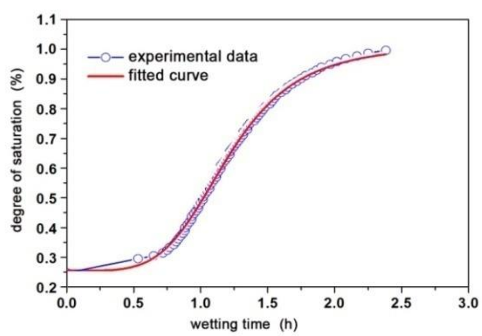

Figure 10. Wetting test for the strongly fragmented two mica-quartz schist sample

According to the wetting test (Fig. 10), $Sr_{sat} = 1$ and $Sr_{res} = 0.27$. The hydraulic parameters could be simplified as $\mathrm{a_d} = \mathrm{a_w}$ and $\mathrm{n_d} = \mathrm{n_w}$, because the water infiltration could be simplified as a monotonous wetting process. With the initial and final degree of saturation and the suction, the parameters could be back-calculated (Table 2).

Table 1: Elasto-plastic parameters

Properties	E	v	$\varphi_{c0} = \varphi_{e0}$ (°)	$\varphi_{cf} = \varphi_{ef}$ (°)	c_0 (KPa)	c_f (KPa)	$c_0{}'$ (KPa)	$c_f{}'$ (KPa)	$\psi_c = \psi_e$ (°)	B_p	B_c	ρ (Kg/m^3)
Chlorite-hornblende	36	0.31	41	41	414	414	-	-	1	0.01	0.02	2910
Chlorite schist	25	0.28	36	38	71	77.4	-	-	1	0.01	0.02	1825

Two-mica quartz schist	0.8	0.26	24	27	64	69	42	46	1	0.01	0.02	1675

Table 2: Hydraulic parameters of two-mica quartz schist and chlorite schist

a_d	n_d	a_w	n_w	Sr_{sat}	Sr_{res}
1.94	3.03	1.94	3.03	1	0.27

3.2.3 Results and analysis

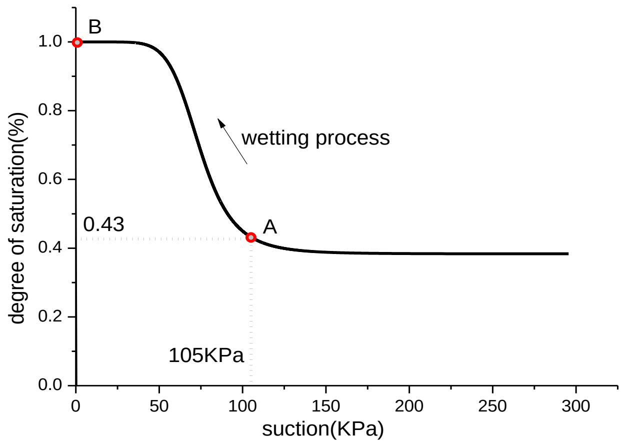

Figure 11. Relationship between suction and degree of saturation during the monotonous wetting process. The segment from point A to point B shows the two mica-quartz schist

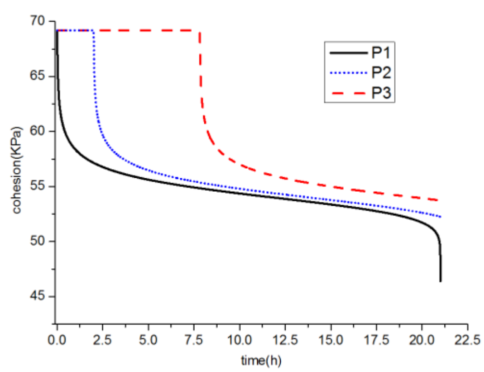

Figure 12. Evolution of apparent cohesion at points P1, P2, and P3

Fig. 11 shows the suction-degree of saturation curve for the monotonous wetting process. The segment from point A to point B corresponds to the two mica-quartz schist. At point A, the suction was 105 kPa, corresponding to a degree of saturation of 43%. At point B, the suction was 0, corresponding to a degree of saturation of 100%. For a detailed comparison of apparent cohesion and second order work at different positions along the slope, three material points, P1, P2, and P3, were selected on the top surface, the middle of the slope, and the toe of the slope, respectively (Fig. 13a). The decrease of apparent cohesion was induced by the decrease in suction, according to Equation 12. Clearly, the material at point P1 underwent an immediate decrease of apparent cohesion from 69 to 46 kPa, and points P2 and P3 showed a delay in strength reduction (Fig. 12) because of infiltration at different altitudes; therefore, the homogeneous initial suction began to decrease at different times.

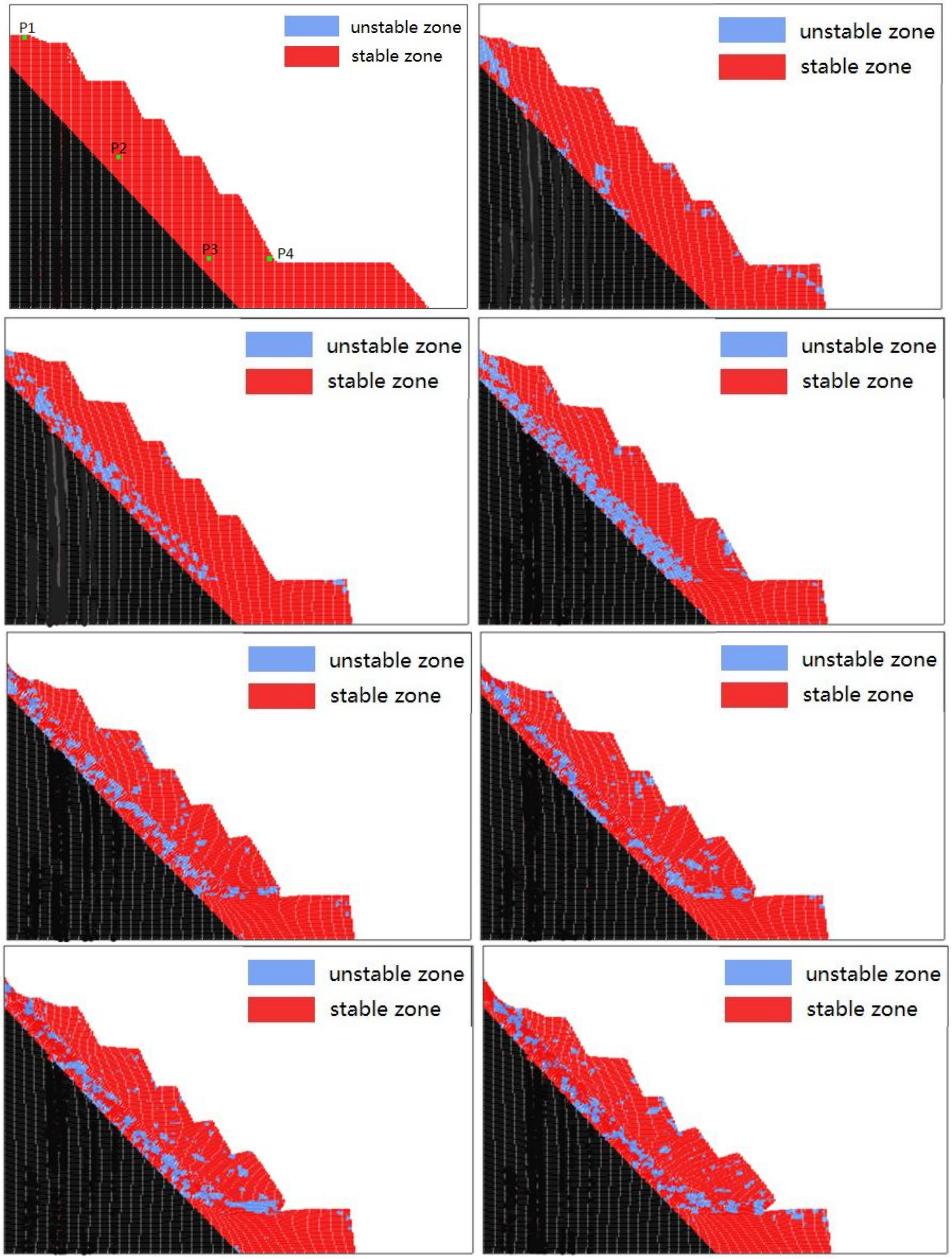

Figure 13. Stable zones (red) and the development of unstable zones (blue) during the consistent evolution of the rockslide. (a) Initial configuration after gravity initialization; (b) unstable zones after excavation; (c) water infiltration after *12 h;* (d) Water infiltration after *25 h*,$D^2W_{norm} = 0$; (e) slip configuration after*1s*; (f) slip configuration after *3s;* (g) Slip configuration after *5s;* (h) Slip configuration after *7s*

Fig. 13 shows the development of unstable zones under excavation and water infiltration conditions, and the entire rockslide process at various elapsed times. The unstable zones correlate to a negative local second order work calculated by Equation 9a. Unstable zones first concentrate at material points on the top and toe of the slope, because of excavation at the toe (Fig. 13b). Compared with Fig. 15, d^2w_{norm} at points P1 and P2 indicates a slight decrease, and point P3 shows a more significant decrease at 38 h, when excavation on the toe was performed. However, this change did not induce any clear instability, and all three material points remained stable. During the subsequent 46 hours after excavation, values of d^2w_{norm} remained positive and constant, and that of point P3 progressively increased. When water infiltration occurred on the top surface, the d^2w_{norm} of points P1, P2, and P3 started to decrease quickly, and became zero at 92.8 h, 102 h, and 109 h, respectively, according to Fig. 15, which signifies failures at these points. Fig. 13 (c and d) also shows that unstable zones developed quickly along the major geological discontinuity under infiltration conditions, but few unstable zones appeared in the upper slide bodies because of the very low permeability ($k_2 = 1 \times 10^{-8}$ cm/s).

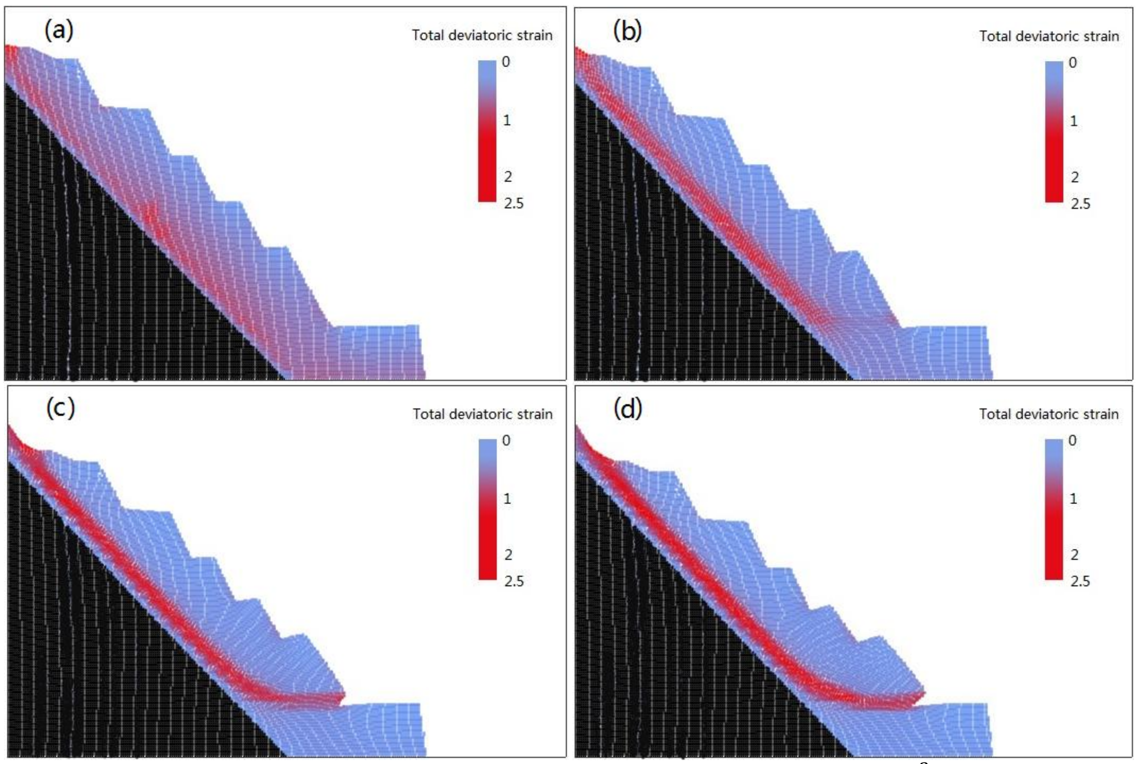

Figure 14. Evolution of the shear strain band: (a) after excavation; (b) global failure, $D^2W_{norm} = 0$; (c) slip configuration after *5s*; and (d) slip configuration after *7s*

After failure, the simulated rockslide involved continuous, large deformation (Fig. 13e-h). The shear strain band developed first along the major discontinuity, and then a horizontal band appeared between that and the toe of the slope (Fig. 14). The shear strain band became well developed and failure occurred. Clearly, the rockslide developed owing to large deformation along the major discontinuity and at the toe of the slope. Most zones of the upper chlorite schist remained stable during the elastic stage, and then slipped as one mass along the two-mica quartz schist weak zone. The simulation results were therefore consistent with the real case.

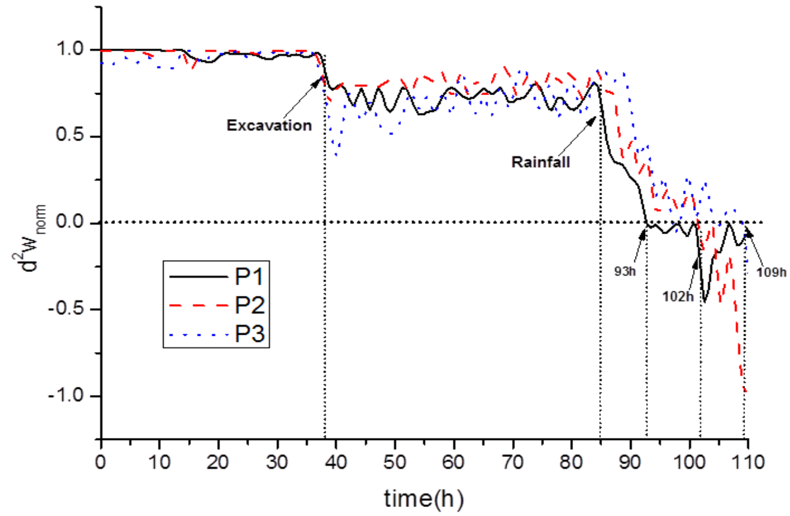

Figure 15. Evolution of normalized local second order work with time

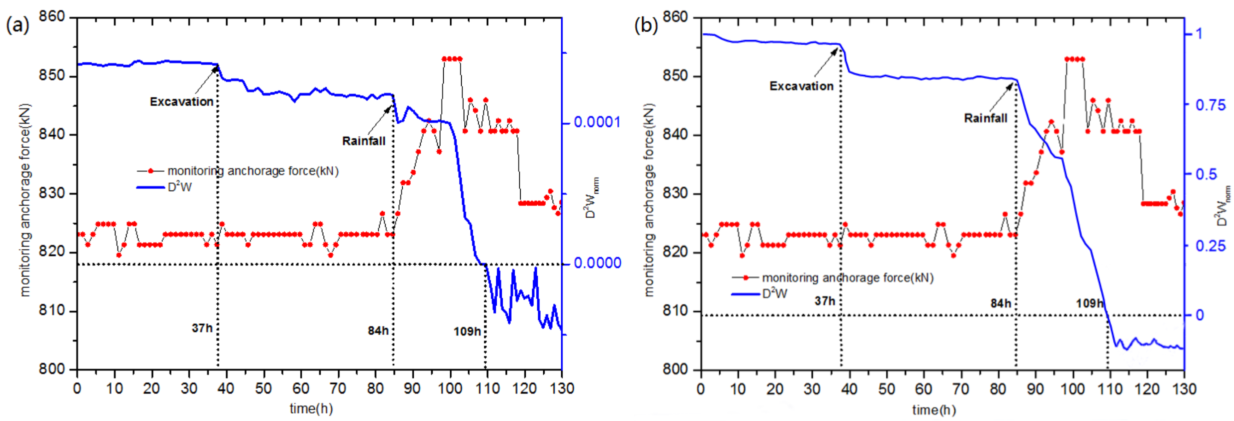

Figure 16. Evolution of monitoring anchorage force and normalized global second order work, computed according to (a) equation (10) and (b) equation (11)

Fig. 16 illustrates the evolution of the normalized global second order work calculated according to equations (10) and (11), respectively, and compares them with that of the monitored anchorage force. The excavation at 37 h evoked a slight decrease in D^2W_{norm}, correlated with the trend in d^2w_{norm}. However, the mining activity on the toe of the slope did not influence significantly the stability of the slope, and the curve of anchorage force only showed a slight fluctuation before returning quickly to its previous value. The second significant decrease of D^2W_{norm} was caused by water infiltration at 84–105 h. During the rainfall, D^2W_{norm} decreased quickly with failure along the major discontinuity, and became zero at 109 h, after 4 h of rainfall. At the same time, the anchorage force reached a peak of 852 kN, because the decreasing apparent cohesion was not sufficient to resist the increasing sliding force. The anchorage force then decreased to 841 kN, corresponding to a local slide between the benches at 502 and 490 m elevation. Subsequently, the anchorage force showed a second decrease, to a value of 825 kN, at the point of global failure and the rockslide event. The trend of D^2W_{norm} mainly correlates to that of the monitoring data, and both prove that the October 31, 2016 rockslide was induced by rainfall. Regarding the comparison between the two global second order work, both of them presented two sudden decreases during excavation and rainfall were exerted, and both of them vanished at 109 h. It was evident that their evolutions were mainly similar, because the numerators in equations (10) and (11) were identical. However, the value of the former decreased with the finer mesh, that of the later varied between 1 and 0 in any case, and presented less fluctuation. The normalized global second order work computed by equation (11) can theoretically be used as a safety factor for analyzing the global stability of a boundary value problem.

4. Conclusions

In this study, we considered a recent rockslide in the Nanfen open-pit iron ore mine that was successfully predicted using the real-time monitoring system. The core of the monitoring system was the CRLD cable, whose properties, the constant resistance and large deformation, made the disaster prediction possible, during the occurrence of landslides. The CRLD cable can monitor and reflect increasing sliding force and the degradation of the mechanical properties of geomaterials in deep strata, despite of the triggering factors, and the successful predictions of the excavation-induced rockslide in 2011 and the rainfall-induced rockslide in 2016 are good evidences. This monitoring system has exhibited its reliability and generality, and further generalization is thus expected.

Based on in-situ surveys and monitoring data, this rockslide was considered to have been induced by rainfall. Mining activities augmented the instability risk but were not the direct cause of the rockslide. A numerical analysis was performed using the FEMLIP method. An elasto-plastic constitutive model incorporating hydro-mechanical coupling and the second order work criterion was employed in order to solve water infiltration and instability problems. The results were carefully analyzed, comparing with the monitoring data, and several conclusions could be obtained:

1. The evolution of second order work indicated a good correlation with monitoring data, both for the failure mechanism predicted by the local values of second order work and failure time by its global value. Water infiltration induced a decrease in strength of the major geological discontinuity, and a subsequent increase in the anchorage force to support the increasing sliding force due to adjacent sliding bodies. Accordingly, the decrease in the local and global values of second order work was a response to the decreasing geomaterial strength. Finally, water infiltration along the major geological discontinuity prompted the rockslide.
2. Both of the Equations (10) and (11) of the normalized global second order work were implanted in FEMLIP code, and the corresponding results were compared. Equation (11) resulted in a result with less fluctuation, and limited within the range 0 to 1, despite of the mesh. It can be used as a safety factor, more general and more physical than the numerical divergence of the calculation.
3. Differing from the classical method, such as the FDM method, the complete evolution of the rockslide could be simulated in a unified frame using the FEMLIP method, which has been shown more generally as useful for predicting the disaster domain and evaluating the dynamic effect on the retaining wall. The numerical analysis is a good assistant tool for understanding the failure mechanism and predicting landslides.

This research suggests that subsequent mining activities should be undertaken with more care, and geological discontinuities with low strength and high permeability should be avoided as much as possible. Geological surveys and monitoring measures should also be carefully consulted. These results have to be compared with some adequate numerical models to fully understand both the failure mechanisms and the critical parameter values inducing the catastrophic instability.

In addition, the instability of rock slopes usually proceeds with the breakage of intact rock bridges. The description of this discontinuous phenomenon using the FEMLIP method is worth being considered. By implementing the level-set functions, widely used in X-FEM, the FEMLIP method can be extended to solve the issues of discontinuous media.

References

Abe, K., Soga, K., and Bandara, S.: Material point method for coupled hydromechanical problems, Journal of Geotechnical and Geoenvironmental Engineering, 140(3), 04013033, 2013.

Arairo, W., Prunier, F., Djéran-Maigre, I., and Darve, F.: A new insight into modeling the behavior of unsaturated soils. International Journal for Numerical and Analytical Methods in Geomechanics, 37(16), 2629-2654, 2013.

Bandara, S., Ferrari, A., and Laloui, L.: Modelling landslides in unsaturated slopes subjected to rainfall infiltration using material point method, International Journal for Numerical and Analytical Methods in Geomechanics, 40(9), 1358-1380, 2016.

Barnichon, J.D.: Finite element modelling in structural and petroleum geology, Ph.D. Thesis, University of Liege, 1998.

Bishop, A.W.: Principle of effective stress, Teknisk Ukeblad, 106(39), 859-863, 1959.

Cascini, L., Cuomo, S., Pastor, M., Sorbino, G., and Piciullo, L.: SPH run-out modeling of channelized landslides of the flow type, Geomorphology, 214(2), 502-513, 2014.

Chen, H., Dadson, S., and Cui, Y.: Recent rainfall-induced landslides and debris flow in northern Taiwan, Geomorphology, 77(1-2), 112-125, 2006.

Cuomo, S., Prime, N., Iannone, A., Dufour, F., Cascini, L., and Darve, F.: Large deformation FEMLIP drained analysis of a vertical cut, Acta Geotechnica, 8(2), 125-136, 2013.

Darve, F. and Servant, G.: Fundamental of constitutive equations for geomaterials, Degradations and instabilities in geomaterials, Springer Vienna, 461, 1-33, 2004.

Darve, F., Servant, G., Laouafa, F., and Khoa, H.D.V.: Failure in geomaterials : continuous and discrete analyses, Computer Methods in Applied Mechanics and Engineering, 193(27-29), 3057-3085, 2004.

Dong, H.K., Ivan, G., and Arumugam, B.: Back analysis of a natural jointed rock slope based on the photogrammetry method, Landslides, 12(1), 147-154, 2015.

Duriez, J., Darve, F., and Donze, F.V.: Incrementally non-linear plasticity applied to rock joint modeling, International Journal for Numerical and Analytical Methods in Geomechanics, 37(5), 453-477, 2011.

Feng, M., Fredlund, D.G.: Hysteretic influence associated with thermal conductivity sensor measurements, In Proceedings from Theory to the Practice of Unsaturated Soil Mechanics in Association with the 52nd Canadian Geotechnical Conference and the Unsaturated Soil Group, Regina, Sask, 14(2), 14–20, 1999.

Harlow, F.H.: The particle-in-cell computing method for fluid dynamics, Computer Methods in Physics, 3, 319-343, 1964.

He, M.C.: Real-time remote monitoring and foresting system for geological disasters of landslides and its engineering application (in Chinese), Chinese Journal of Rock Mechanics and Engineering, 28(6), 1081-1090, 2009.

He, M.C., Gong, W.L., Wang, J., Qi, P., Tao, Z.G., Du, S., and Peng, Y.Y.: Development of a novel energy-absorbing bolt with extraordinarily large elongation and constant resistance, International Journal of Rock Mechanics and Mining Sciences, 67(67), 29-42, 2014.

Hill, R.: A general theory of uniqueness and stability in elastic-plastic solids, Journal 1 of the Mechanics and Physics of Solids, 6, 236-249, 1958.

Huang, D., Cen, D.F., Ma, G.W., and Huang, R.Q.: Step-path failure of rock slopes with intermittent joints, Landslides, 12(5), 911-926, 2015.

James, J., Conca, A.B., and Judith Wright, A.B.: The UFA method for rapid, direct measurements of unsaturated transport properties in soil, sediment, and rock, Australian Journal of Soil Research, 36, 291-315, 1998.

Khoa, H.D.V., Georgopoulos, I.O., Darve, F., and Laouafa, F.: Diffuse failure in geomaterials: experiments and modelling, Computers and Geotechnics, 33, 1-14, 2006.

Laouafa, F., Prunier, F., Daouadji, A., Al Gali, H., and Darve, F.: Stability in geomaterials, experimental and numerical analyses, International Journal for Numerical and Analytical Methods in Geomechanics, 35, 112-139, 2011.

Li, Z.H., Dufour, F., and Darve, F.: Hydro-elasto-plastic modelling with a solid/fluid transition, Computers and Geotechnics, 75, 69-79, 2016.

Li, Z.H., Dufour, F., and Darve, F.: Modelling rainfall-induced mudflows using FEMLIP and a unified hydro-elasto-plastic model with solid-fluid transition, European Journal of Environmental and Civil Engineering, 22(4), 491-521, 2018a.

Li, Z.H., Jiang, Y.J., Tao, Z.G., He, M.C.: Monitoring prediction of a rockslide in an open-pit mine and numerical analysis using a material instability criterion, Bulletin of Engineering Geology and Environment, published online, 2018b.

Li, Z.H., Jiang, Y.J., Lv, Q., Sousa L., He, M.C.: Consistent modeling of a catastrophic flowslide at the Shenzhen

landfill using a hydro-elasto-plastic model with solid-fluid transition. Acta Geotechnica, 13(6): 1451-1466, 2018c.
Lignon, S., Laouafa, F., Prunier, F., Khoa, H.D.V., and Darve, F.: Hydro-mechanical modelling of landslides with a material instability criterion, Géotechnique, 59(6), 513-524, 2009.
Marcelo, A., Llano-Serna, M.F., and Dorival, M.P.: An assessment of the material point method for modeling large scale run-out processes in landslides, Landslides, 13(5), 1057-1066, 2016.
Ministry of Water Resources and Electric Power of People's Republic of China, Code for Engineering Geological Investigation of Water Resources and Hydropower GB50487-2008 (in Chinese), 2008.
Moresi, L., Dufour, F., and Muhlhaus, H.B.: Mantle convection modeling with viscoelastic/brittle lithosphere: numerical methodology and plate tectonic modeling, Pure and Applied Geophysics, 159(10), 2335-2356, 2002.
Moresi, L., Dufour, F., and Muhlhaus, H.B.: A Lagrangian integration point finite element method for large deformation modelling of viscoelastic geomaterials, Journal of Computational Physics, 184(2), 476-497, 2003.
Nicot, F., and Darve, F.: Diffuse and localized failure modes: Two competing mechanisms, International Journal for Numerical and Analytical Methods in Geomechanics, 35(5), 586-601, 2011.
Parlange, J.Y.:Water transport in soils, Annual Revision of Fluid Mechanics, 12, 77–102, 1980.
Prime, N., Dufour, F., and Darve, F.: Unified model for Geomaterial solid/fluid states and the transition in between, Journal of Engineering Mechanics, 140(6), 682-694, 2013.
Prunier, F., Laouafa, F., Lignon, S., and Darve, F.: Bifurcation modelling in geomaterial : From the second-order work criterion to spectral analyses, International Journal for Numerical and Analytical Methods in Geomechanics, 33(9), 1169-1202, 2009.
Prunier, F., Chomette, B., Brun, M., and Darve, F.: Designing geotehcnical structures 1 with a proper stability criterion as a safty factor, Computers and Geotechnics, 71, 98-114, 2016.
Regmi, A.D., Yoshida, K., Dhital, M.R., and Devkota, K.: Erratum to: Effect of rock weathering, clay mineralogy, and geological structures in the formation of large landslide, a case study from DumreBesei landslide, Lesser Himalaya Nepal, Landslides, 9(2), 299-301, 2012.
Soga, A., Alonso, E., Yerro, A., Kumar, K., and Bandara, S.: Trends in large deformation analysis of landslide mass movements with particular emphasis on the material point method, Géotechnique, 1-26, 2016
Sun, D.X., Tao, Z.G., Fan, L.J., and Feng, X.R.: Stability assessment and sensibility analysis of Nanfen open-pit mine slope (in Chinese), Metal Mine, 5, 57-60, 2011.
Tu, X.B., Kwong, A.K.L., Dai, F.C., Tham, L.G., and Min, H. Field monitoring of rainfall infiltration in a loess slope and analysis of failure mechanism of rainfall-induced landslides, Engineering Geology, 105(1-2), 134-150, 2009.
Van Eekelen, H.A.M.: Isotropic yield surfaces in three dimensions for use in soil mechanics, International Journal of Numerical and Analytical Methods in Geomechanics, 4, 89-101, 1980.
Van Genuchten, M.T.: A closed-form equation for predicting the hydraulic conductivity of unsaturated soils, Soil Science Society of America Journal, 44, 892-898, 1980.
Wang, J.J., Zhang, H.P., Liu, T.: Determine to slip surface in waterfront soil slope analysis, Advanced Materials Research, 378-379, 466-469, 2011.
Yang, F., Hou, K.P., and Xie, Y.L.: Mechanical parameters determination method for strongly weathered mica-quartz schise (in Chinese), Journal of Chang'an University, 32(2), 29-38, 2012.
Zhang, K., Tan, P., Ma, G.W., and Can, P.: Modeling of the progressive failure of an overhang slope subject to differential weathering in Three Gorges Reservoir, China, Landslides, 13(5), 1303-1313, 2016.